Sciortino, Giuseppe; Lihi, Norbert; Czine, Tamás; [et al.]. «Accurate prediction of vertical electronic transitions of Ni(II) coordination compounds via time dependent density functional theory». International Journal of Quantum Chemistry, Vol. 118, Issue 16 (August 2018), p. e25655. DOI 10.1002/qua.25655

Accurate prediction of vertical electronic transitions of Ni(II) coordination compounds via Time Dependent DFT

Giuseppe Sciortino,[1,2] Norbert Lihi,[3,]* Tamás Czine,[4] Jean-Didier Maréchal,[1] Agustí Lledós,[1,]* Eugenio Garribba[2,]*

[1]Departament de Química, Universitat Autònoma de Barcelona, 08193 Cerdanyola del Vallés, Barcelona, Spain

[2]Dipartimento di Chimica e Farmacia, Università di Sassari, Via Vienna 2, I-07100 Sassari, Italy

[3]MTA-DE Redox and Homogeneous Catalytic Reaction Mechanisms Research Group, University of Debrecen, H-4032 Debrecen, Hungary

[4]Department of Inorganic and Analytical Chemistry, University of Debrecen, H-4032 Debrecen, Hungary

Correspondence to

Norbert Lihi, MTA-DE Redox and Homogeneous Catalytic Reaction Mechanisms Research Group, University of Debrecen, H-4032 Debrecen, Hungary. E-mail: lihi.norbert@science.unideb.hu

Agustí Lledós, Departament de Química, Universitat Autònoma de Barcelona, 08193 Cerdanyola del Vallés, Barcelona, Spain. E-mail: agusti@klingon.uab.es

Eugenio Garribba, Dipartimento di Chimica e Farmacia, Università di Sassari, Via Vienna 2, I-07100 Sassari, Italy. E-mail: garribba@uniss.it

Funding information

This work is supported by: the ÚNKP-17-3 New National Excellence program of the Ministry of Human Capacities; the EU and co-financed by the European Regional Development Fund under the project GINOP-2.3.2-15-2016-000; the Hungarian Scientific Research Fund (K 124983); the Spanish MINECO (project CTQ2014-54071-P); Universitat Autònoma de Barcelona; Fondazione di Sardegna.

ABSTRACT

TD-DFT calculations are completed for five Ni(II) complexes formed by polidentate peptides to predict the electronic absorption spectrum. The ligands examined were glycyl-glycyl-glycine (GGG), glycyl-glycyl-glycyl-glycine (GGGG), glycyl-glycyl-histidine (GGH), glycyl-glycyl-cysteine (GGC) and triethylenetetramine (trien). Fifteen functionals and two basis sets were tested. On the basis of the mean absolute percent deviation (MAPD) the ranking among the functionals is: HSE06 ~ MPW1PW91 ~ PBE0 > ω-B97x-D ~ B3P86 ~ B3LYP ~ CAM-B3LYP > PBE ~ BLYP ~ BP86 > TPSS > TPSSh > BHandHLYP > M06 >> M06-2X. Concerning the basis sets, the triple-ζ *def2*-TZVP performs better than the double-ζ LANL2DZ. With the functional HSE06 and basis set *def2*-TZVP the MAPD with respect to the experimental λ_{max} is 1.65% with a standard deviation of 1.26%. The absorption electronic spectra were interpreted in terms of vertical excitations between occupied and virtual MOs based on Ni-*d* atomic orbitals. The electronic structure of the Ni(II) species is also discussed.

KEYWORDS

Nickel, UV-Vis spectroscopy, TD-DFT, peptides, electronic structure

1. INTRODUCTION

The prediction of the structure, reactivity and stability of a chemical compound has always been a big challenge not only in chemistry, but also in physics and biology. During the past decades, computational methods allowed the chemists to calculate the structure, molecular properties and energetics of many chemical species. Among these methods, density functional theory (DFT)[1] has reached an enormous popularity and many reviews have been published.[2], [3], [4], [5], [6], [7], [8], [9], [10] The main advantage of DFT is that many packages are available, commercially or free of charge, which allow one calculations on large molecules in an user friendly manner; nowadays, molecules with more than one hundred atoms can be treated routinely. At the moment, many molecular properties of a chemical compound, such as the 3D structure, can be predicted with great accuracy. Concerning the spectroscopic properties, whereas NMR and EPR can be calculated successfully for a large number of molecules,[11], [12] the prediction of IR and optical spectra (UV-vis, CD, MCD) is possible only qualitatively and a quantitative agreement has not been obtained yet for transition metal containing molecules.[3], [13]

UV-vis spectroscopy is probably the simplest instrumental method to study the electronic transitions of metal complexes. Even if UV-vis usually gives less information than CD-spectroscopy, the energy of *d-d* absorptions could be related to the oxidation states, geometry and electronic structure of a chemical species in the absence of chiral centers as well. Time-dependent density functional theory (TD-DFT),[14] an extension of DFT, is a widely used technique to understand the structure and electronic transitions of organic and inorganic compounds and to predict the absorption or electronic circular dichroism spectra that could directly be compared to the experimental results. Moreover, the prediction of the UV-vis spectra using TD-DFT is frequently discussed and a number of benchmarks and reviews are available in this field.[3, 15] Based on this fact, if metal coordination compounds are taken into account, comprehensive investigations have been published focusing on Pt(II) and Ir(III) complexes,[16] and on the first-row transition metal complexes, for example formed by Zn(II) and Cu(II).[17] Visible circular dichroism studies have been performed with some tripeptides and a set of empirical rules was developed to put in relationship the appearance of UV-vis and CD spectra.[18] The effect of solvation as specific correction for the excited states has also been widely studied,[15a, 15c, 19] and a comprehensive study is available, focusing on the electronic structure and spectroscopic properties of inorganic compounds.[20] Up to now, however, the applicability of TD-DFT techniques is often limited to the qualitative prediction of the absorption spectra. In other words, in many cases it is possible to predict the origin of the experimental absorptions and attribute them to *d-d*, MLCT, LMCT or intraligand transitions, but it is not possible to calculate the exact wavelength of these bands and often very large percent deviations from the experimental values are observed (see, for example, ref. [21] for vanadium complexes).

The coordination chemistry of Ni(II) ion is widely investigated, in particular in the field of first-row transition metals catalyzed reactions, due to the actual attempts to replace precious metals with high cost and toxicity with nickel. Ni has received particular interest in several catalytic processes such as cross-coupling, Heck reaction, oligomerizations and reductive coupling due to its simple achievable oxidative addition and to the number of readily available oxidation states (I and III, beside the 'usual' II).[22] Moreover, because of its redox properties and the oxidizing power of its high valence states, nickel presents promising application in water oxidation reaction.[23] The interested reader could easily find excellent reviews and books on these topics.[22, 24] Herein, we are focusing our attention on the electronic spectra of this metal ion. Three coordination environments are characteristic for nickel(II), namely the octahedral, tetrahedral and square-planar geometry. In the presence of weak field ligands, octahedral complexes are formed with a paramagnetic behavior (spin state $S = 1$); in contrast, square-planar geometry is stabilized by strong field ligands or compounds with low symmetry, resulting in diamagnetic complexes (spin state $S = 0$). When the ligands are not strong enough to cause spin pairing or the formation of square-planar geometry is hindered because of steric requirements, tetrahedral nickel(II) complexes could be formed.[25]

Peptides are effective ligands for binding metal ions and a number of reviews have been published on the characterization of these interactions.[26] From coordination chemistry point of view, the terminal amino- and carboxylate groups are the primary metal binding sites, even if the donor atoms in the side chains can also make significant contribution to the metal binding resulting in a great diversity of complex formation processes. Probably, the most important amino acids containing strongly coordinating side chains for nickel are histidine and cysteine. Ni(II) is able to bind to these donor groups and, with the help of appropriate anchoring groups, the metal ion can induce the deprotonation and coordination of peptide nitrogen (N^-) resulting in square-planar complexes.[26d] For example, histidine in the third position from the amino terminus is responsible for the high nickel(II) binding affinity of human serum albumin (the XYHisZ sequence, where X, Y and Z are three amino acids of variable identity, is often named as ATCUN – Amino Terminal CuNi motif – binding site[27]). More than 90% of Ni(II) in the blood is transported by albumin bound at ATCUN site with the coordination mode (NH_2,N^-,N^-,N_{His}).[27] Similar effect has been observed in the case of copper(II), and this is the reason for using nickel(II) as a diamagnetic probe in the NMR studies of Cu(II) containing metalloenzymes.[28] Moreover, nickel(II) has also a biological role in the case of bacteria such as *helicobacter pylori*, in which its presence is indispensable for the bacteria to survey the extreme acidic environment of stomach.[29] A particular type of superoxide dismutase (SOD) enzyme also contains nickel(II).[30] The distortion of the geometry (so-called pseudoplanar) has been observed in the case of the interaction of Ni(II) with salen-type Schiff base ligands.[31] This family of molecules is frequently investigated because of the great variety of applications such as catalytic, industrial, optical or medical, and DFT studies were also carried out.[32]

For all the systems mentioned above, the characterization of the Ni(II) species is often performed through UV-vis spectroscopy but, to the best of our knowledge, a comprehensive TD-DFT study on nickel(II) complexes has not previously been reported. Based on this fact, DFT and TD-DFT studies were performed with nickel(II) complexes where several peptides (glycyl-glycyl-glycine (abbreviated as GGG), glycyl-glycyl-glycyl-glycine (abbreviated as GGGG), glycyl-glycyl-histidine (abbreviated as GGH) and glycyl-glycyl-cysteine (abbreviated as GGC)) and triethylenetetramine (abbreviated as trien) were used as ligands. The peptides and trien are able to form square-planar nickel(II) complexes. The structures of the investigated ligands are shown in Scheme 1. The aim of this study was to find the best functional and basis ser for predicting the UV-vis spectra of these kind of complexes and provide information useful for their interpretation and assignment of the absorptions.

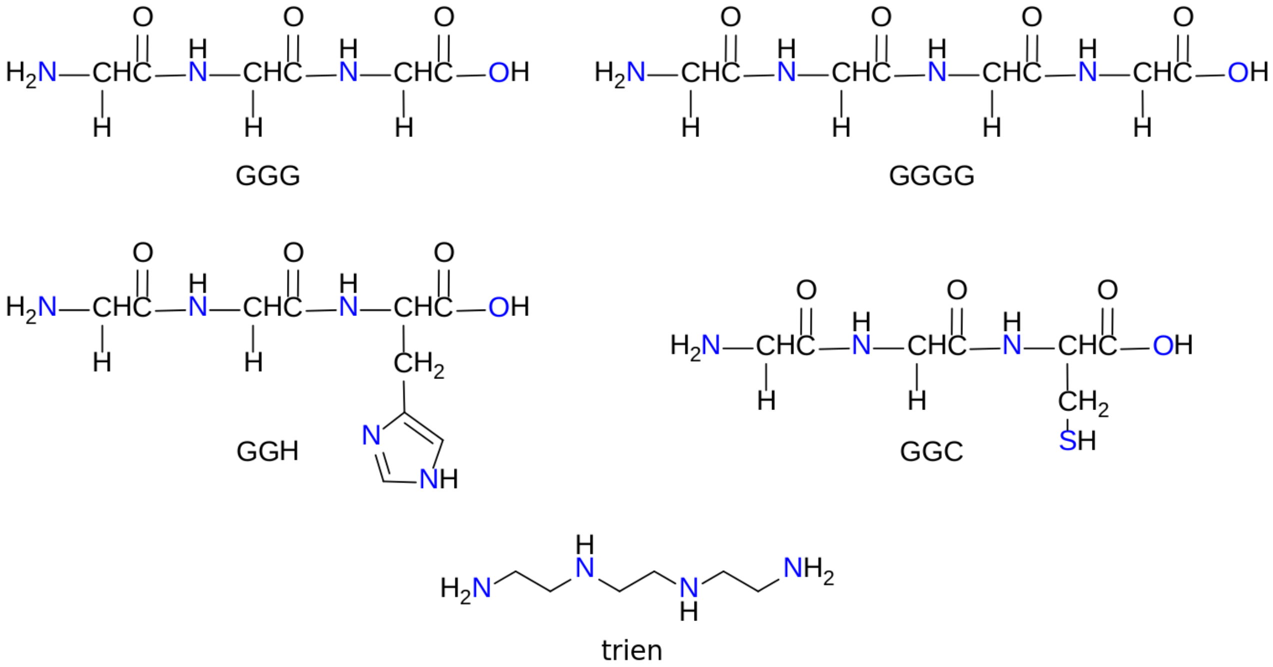

SCHEME 1 Structural formulae of the ligands. The potential donor atoms are highlighted in blue.

2. EXPERIMENTAL AND COMPUTATIONAL DETAILS

Materials. All of the investigated peptides (see Scheme 1) were purchased from Bachem AG (Switzerland) and the concentration of peptide stock solutions were checked by pH-potentiometric titrations. The nickel(II) stock solution was prepared from analytical grade reagent $NiCl_2$ and its concentration was checked gravimetrically *via* the precipitation of oxinate.

Spectroscopic method. UV-visible spectra of the nickel(II) complexes were recorded from 200 to 1000 nm on a PerkinElmer Lambda 25 scanning spectrophotometer.

Density functional theory (DFT) and time-dependent density functional theory (TD-DFT) calculations. All ground electronic state geometry optimization and harmonic frequency of the studied complexes were computed through Gaussian 09 software[33] at DFT level of theory, using the hybrid Becke three-parameter B3P86 functional[34], [35] combined with the triple-ζ *def2*-TZVP basis-set. The solvent effect was taken into account adopting the Polarizable Continuum Model (PCM) by Tomasi and coworkers[36] for water. These conditions have been successfully applied and discussed in the literature for the geometry prediction of first-row transition-metal complexes.[37], [38]

The electronic transitions were calculated at TD-DFT level of theory, using PCM for water and starting from the geometries optimized for the ground electronic state. Fifteen functionals were tested: functionals based on the generalized gradient approximations (GGA), including B3LYP,[34], [39] B3P86,[34-35] CAM-B3LYP,[40] ω-B97x-D,[41] MPW1PW91,[42] HSE06,[43] PBE0,[44] BHandHLYP,[33] the meta GGA functionals TPSSh,[45] M06,[46] M06-2X,[46] and the pure BLYP,[39, 47] PBE,[44] BP86[35, 47] and TPSS[45a] functionals, all of them combined with the basis sets LANL2DZ and *def2*-TZVP. The representation of the electronic spectra was generated with Gabedit software,[48] and the molecular orbitals involved in the transitions were simulated performing a Mulliken population analysis (MPA) with Gaussian 09 at the same level of theory used for the TD-DFT calculations and identified *via* the AOMix package (vers. 6.52).[49]

3. RESULTS AND DISCUSSION

Nickel(II) complexes of the investigated peptides. In order to predict the electronic structure of the nickel(II) peptide complexes, some widely investigated model systems were chosen. The nickel complexes of GGG, GGC, GGH and GGGG have also been characterized and stability constants of the different species are summarized in Table 1. Table 1 contains the overall stability constants ($\log\beta_{pqr}$), where β_{pqr} is defined as $\beta_{pqr} = [Ni_pH_qL_r]/[Ni]^p[H]^q[L]^r$. The negative signs for protons indicates either hydroxide ligands or the dissociation of groups that do not deprotonate in the absence of Ni(II) coordination; for this type of complexes the negative sign can be related to the deprotonation (and coordination) of the amide groups through the N^- donor (i.e., H_{-1} indicates the deprotonation of only one amide group, H_{-2} the deprotonation of two amide groups and so on).

TABLE 1 Stability constants ($\log\beta_{pqr}$) of the nickel(II) peptide complexes.

$\log\beta_{pqr}$	GGG^a	GGGG^b	GGH^c	GGC^d
NiL	3.75	3.65	4.76	
NiL_2	6.77	6.55		
NiHL			11.33	13.67
$NiH_{-1}L$	−5.45	−4.45		
$NiH_{-2}L$	−12.85	−12.65	−6.93	−5.36
$NiH_{-3}L$		−20.90		

[a]Data are taken from ref. [50].
[b]Data are taken from ref. [51].
[c]Data are taken from ref. [52].
[d]Data are taken from ref. [53].

Based on the data in Table 1, the speciation curves of the Ni(II):GGGG and Ni(II):GGC systems are depicted in Figure 1.

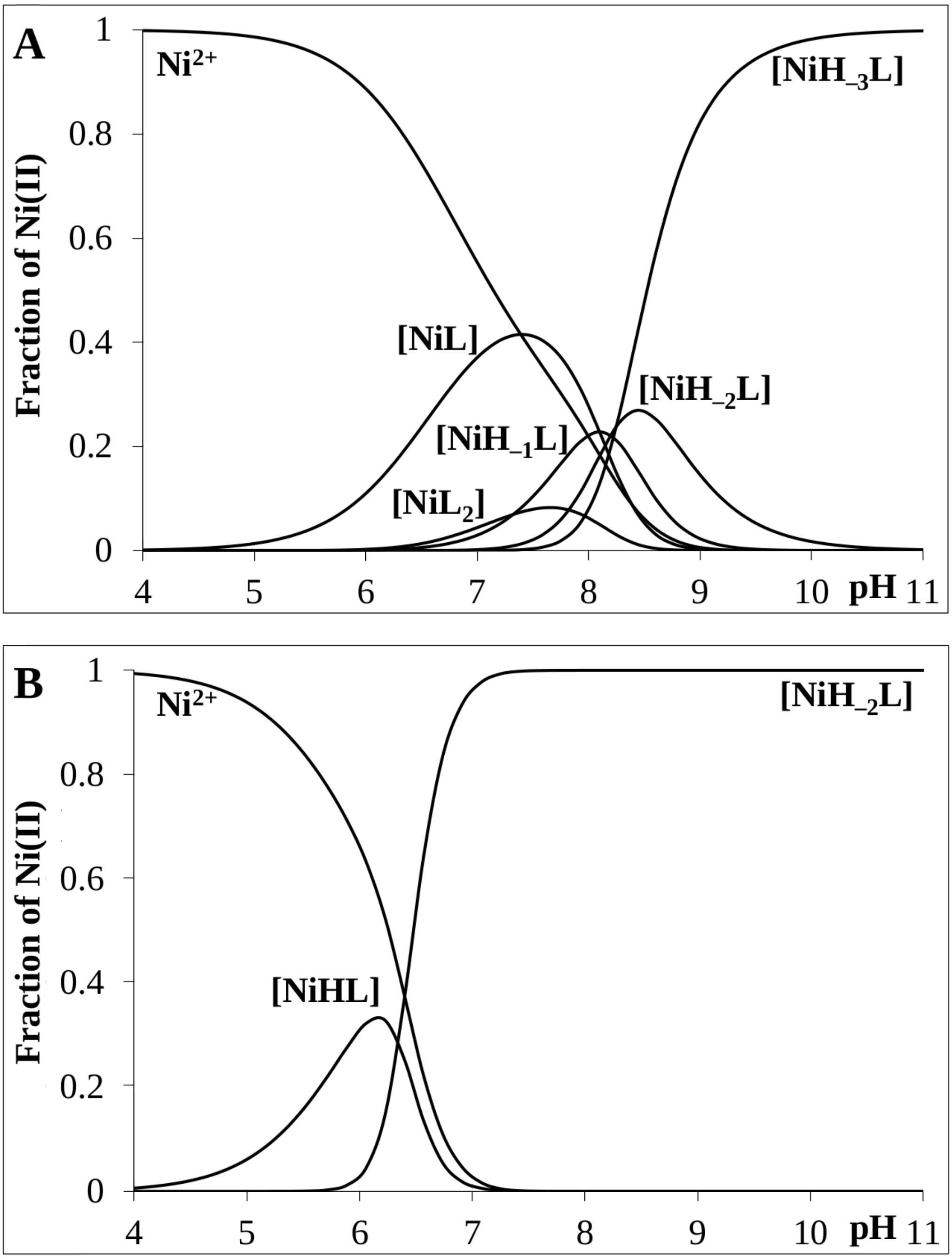

FIGURE 1 Concentration distribution curves formed in the nickel(II):GGGG (A) and nickel(II):GGC (B) systems at 1:1 metal to ligand ratio and Ni(II) concentration of 3 mM.

From Figure 1 it is clear that two types of complex formation processes could be distinguished. In the case of GGG and GGGG containing systems, stepwise complex formation occurs *via* the existence of partial amide bonded species such as NiL, $NiH_{-1}L$, $NiH_{-2}L$ and $NiH_{-3}L$ (this latter observed only with GGGG), respectively. For $NiH_{-2}L$ formed by GGG the equatorial coordination is (NH_2,N^-,N^-,COO^-), whereas for $NiH_{-3}L$ formed by GGGG it is (NH_2,N^-,N^-,N^-). In contrast, the peptides with strongly coordinating side chains, such as GGC and GGH, show different complex formation processes. Namely, the NiHL species is only a minor species with (NH_2,N_{His}) or (NH_2,S^-) coordination environment, and the lack of NiL and $NiH_{-1}L$ strongly suggests the cooperative deprotonation and coordination of two adjacent amide groups in $NiH_{-2}L$, resulting in fully occupied coordination sphere *via* the (NH_2,N^-,N^-,N_{His}) or (NH_2,N^-,N^-,S^-) donor set above pH 7.

For the TD-DFT calculations the species which reach the maximum value of concentration in aqueous solution ($NiH_{-2}L$ and $NiH_{-3}L$ for GGC and GGGG, see Figure 1, and $NiH_{-2}L$ for GGG and GGH) were chosen. In the system with triethylenetetramine, the major species is $[Ni(trien)]^{2+}$ with (NH_2,NH,NH,NH_2) equatorial coordination.

Geometry optimization. During our work, we were focusing on the visible region of the electronic absorption spectrum of five nickel(II) complexes with different ligands (GGG, GGH, GGC, GGGG and trien), donor sets (O, N and S) and total charge (-1, -2, +2). For all these compounds the electronic transitions were simulated at TD-DFT level of theory and the experimental spectrum was recorded as well.

In Figure 2 the optimized structure of the five nickel(II) complexes examined is represented, while Table 2 contains the comparison between the calculated and experimental bond length and angles for three species. Cartesian coordinates obtained from the geometry optimization are also available in Table S1-S5 of Supporting Information.

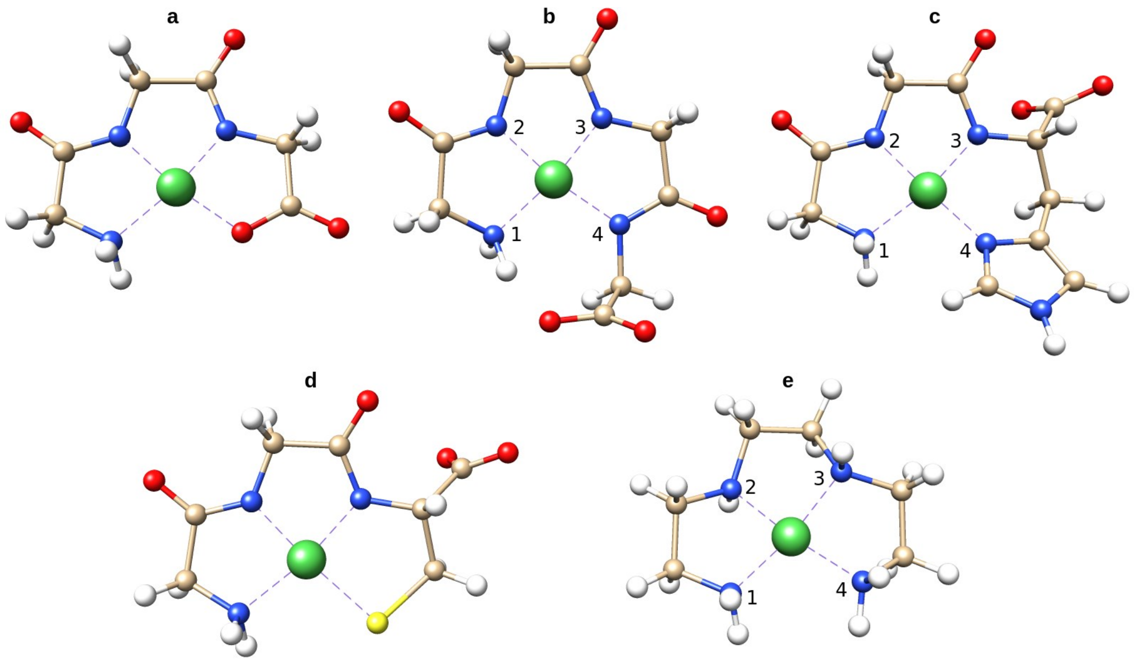

FIGURE 2 DFT optimized structure of the nickel(II) complexes calculated with B3P86 functional and def2-TZVP in water using PCM: (a) $[Ni(H_{-2}GGG)]^-$; (b) $[Ni(H_{-3}GGGG)]^{2-}$; (c) $[Ni(H_{-2}GGH)]^-$; (d) $[Ni(H_{-2}GGC)]^{2-}$ and (e) $[Ni(trien)]^{2+}$. The numbers of the donors reported in Table 2 are also shown.

TABLE 2 Selected bond lengths (Å) and bond angles (degree) for the complexes of $[Ni(H_{-3}GGGG)]^{2-}$, $[Ni(H_{-2}GGH)]^-$ and (e) $[Ni(trien)]^{2+}$ using the functional B3P86 and the basis set *def2*-TZVP.

	$[\mathrm{Ni(H_{-3}GGGG)}]^{2-}$ [a]		$[\mathrm{Ni(H_{-2}GGH)}]^{-}$ [a]		$[\mathrm{Ni(trien)}]^{2+}$	
Parameter[b]	Exptl.[c]	Calcd.	Exptl.[d]	Calcd.	Exptl.[e]	Calcd.
Ni–N(1)	1.93	1.934	1.932	1.954	1.914	1.934
Ni–N(2)	1.84	1.833	1.884	1.827	1.819	1.897
Ni–N(3)	1.83	1.820	1.831	1.881	1.935	1.908
Ni–N(4)	1.87	1.880	1.932	1.904	1.898	1.926
N(1)–Ni–N(2)	85.8	85.82	96.12	84.20	86.59	86.70
N(2)–Ni–N(3)	84.5	85.47	84.30	84.82	91.01	87.60
N(3)–Ni–N(4)	86.8	85.84	84.49	95.05	84.15	85.23
N(4)–Ni–N(1)	102.9	102.90	95.09	96.05	97.05	101.89

[a] As reported in Figure 2, for GGGG and GGH, N(1) is the N-terminal amino group of the peptide, N(2) and N(3) the two deprotonated amide nitrogens, and N(4) the third deprotonated amide N (for GGGG) or the histidyl N (for GGH).

[b] Distances in Å and angles in degrees.

[c] Data are taken from ref. [54] (only two decimal figures for the bond lengths and one for the bond angles were given).

[d] Data are taken from ref. [55].

[e] Data are taken from ref. [56]

As it can be seen from Table 2, a very good agreement has been found with the single-crystal X-ray diffraction parameters using B3P86/*def2*-TZVP level of theory in water (with PCM). The functional B3P86 is frequently used in the literature because of its high degree of accuracy for predicting the structures of transition metal complexes.[38b], [57] On the basis of these results, it is possible to argue that the geometry optimization is reasonably accurate to predict the electronic absorption spectra.

Electronic absorption spectra. The experimental electronic absorption spectra of nickel(II) peptide complexes are shown in Figure 3, while Table 3 contains the spectral data for all of the investigated species. The spectra show an intense absorption band in the region 410-450 nm. This band with a high intensity is a clear-cut evidence for the formation of square-planar complexes. However, the position of the absorption maximum largely depends on the coordinating donor groups. As a representative example, in the case of $[\mathrm{Ni(H_{-2}GGC)}]^{2-}$ this band is observed at 427 nm, while a shoulder with lower intensity is detected at 538 nm. Such a shoulder clearly indicates the presence of the thiolate group in the Ni coordination sphere, as it was described earlier.[58]

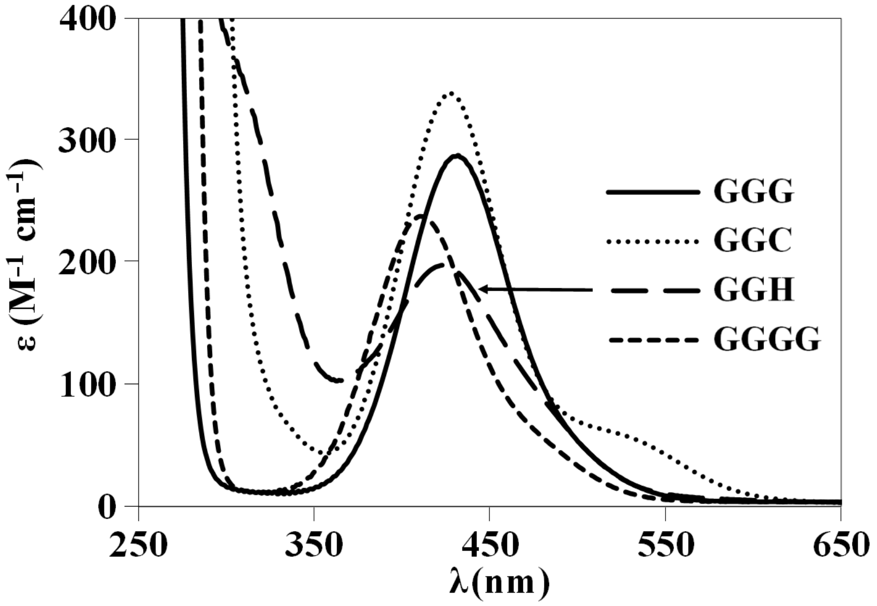

FIGURE 3 UV-vis spectra of the investigated nickel(II)-peptide systems recorded at pH 10.0 at 1:1 metal to ligand ratio and Ni(II) concentration of 2 mM. At this pH the concentration of the Ni(II) complexes reaches its maximum value.

TABLE 3 Absorption spectra data of the investigated Ni(II) complexes.

Complex	Donor set	λ_{max}/nm (ε/M^{-1} cm^{-1})
$[Ni(H_{-2}GGG)]^{-}$	NH_2,N^-,N^-,COO^-	433 (286)
$[Ni(H_{-3}GGGG)]^{2-}$	NH_2,N^-,N^-,N^-	411 (238), 487 (46)^a
$[Ni(H_{-2}GGH)]^{-}$	NH_2,N^-,N^-,N_{His}	425 (198), 307 (353)^a
$[Ni(H_{-2}GGC)]^{2-}$	NH_2,N^-,N^-,S^-	429 (338), 531 (52)^a
$[Ni(trien)]^{2+}$	NH_2,NH,NH,NH_2	445(28)

^{a}Shoulder.

Prediction accuracy of the methods. The benchmark was performed using fifteen functionals based on the generalized gradient approximations (GGA) including the Becke three-parameters hybrid functionals B3LYP and B3P86, the long-range-corrected functional CAM-B3LYP, the functional ω-B97x-D from Chai and Head-Gordon including dispersion, the one-parameter MPW1PW91 with modified Perdew-Wang exchange and correlation, the functionals employing PBE correlation HSE06 and PBE0, the half-and-half functional BHandHLYP, the meta-GGA functional TPSSh including the τ-dependent gradient-corrected correlation, the functionals M06 and M06-2X from the Truhlar group and the pure BLYP, PBE, BP86 and TPSS. All of them have been combined with two basis sets, the double-ζ LANL2DZ and the triple-ζ including polarization *def2*-TZVP in order to evaluate their effect on the quality of the simulation of vertical electronic transitions. The prediction capabilities of the methods were evaluated using the absolute percent deviation (APD), the mean percent deviation (MPD) and the mean absolute percent deviation (MAPD) from the experimental value of the main transition in the spectra (λ_{max}). APD and MAPD are defined as:[59]

$$APD = \left| \frac{\lambda_{max}^{calc} - \lambda_{max}^{exp}}{\lambda_{max}^{exp}} \right| \times 100 \tag{1}$$

$$\mathrm{MAPD} = \frac{1}{N}\sum_{j=1}^{N}\left|\frac{\lambda_{\mathrm{max}}^{\mathrm{calc}}(j) - \lambda_{\mathrm{max}}^{\mathrm{exp}}(j)}{\lambda_{\mathrm{max}}^{\mathrm{exp}}(j)}\right| \times 100 \qquad (2)$$

The value of the percent deviation (PD) was also considered to identify the nature of the error reported for the functionals; in fact, positive values indicate an overestimation, while negative values denote an underestimation of the prediction of transitions in the UV-vis spectrum.

From an analysis of the MAPD values obtained for each functional, tested with the five Ni(II) complexes, it can be observed that the best performances are achieved by the two functionals employing PBE correlation, HSE06 and PBE0, and the Becke one-parameter MPW1PW91. Nevertheless, it is important to note that comparable behavior of PBE0 and MPW1PW91 comes from the minor differences between these functionals because the latter includes only one additional parameter not present in PBE0. On the basis of the MAPD values the following ranking is found: HSE06 ~ MPW1PW91 ~ PBE0 > ω-B97x-D ~ B3P86 ~ B3LYP ~ CAM-B3LYP > PBE ~ BLYP ~ BP86 > TPSS > TPSSh > BHandHLYP > M06 >> M06-2X (see Figure 4b). An analysis of the error dispersion based on the value of the standard deviation allows reaching a similar conclusion, suggesting that the highest accuracy of the benchmark is obtained with the HSE06 functional.

On the basis of the APD values, it can be observed that the functionals can be grouped in three different groups with similar trends, depending on the amount of Hartree-Fock (HF) exchange: a) HSE06 (short range HF exchange 25%, long range HF exchange 0%), MPW1PW91 (25% HF exchange), and PBE0 (25% HF exchange) give results very close to the experimental values; b) ω-B97x-D (short range HF exchange 22.2%, long range HF exchange 100%), B3P86 (20% HF exchange), CAM-B3LYP (short range HF exchange 19%, long range HF exchange 65%), B3LYP (20% HF exchange), TPSSh (10% HF exchange), BLYP (pure DFT), PBE (pure DFT), BP86 (pure DFT) and TPSS (pure DFT) underestimate the position of the electronic transitions and c) BHandHLYP (50% HF exchange), M06 (27% HF exchange) and M06-2X (54% HF exchange) overestimate the experimental bands as it can be seen in Figure 4a. Analyzing the trend of the predictions as a function of the percentage of Hartree-Fock exchange, it can be concluded that the best performances are achieved by the three functionals with an amount of 25% of HF exchange. Larger amount results in an overestimation of the experimental absorptions, smaller amount in an underestimation. Similar tendencies have also been observed in the case of zinc(II) and copper(II) complexes with thiosemicarbazone-type ligands, for which the hybrid functionals with 25% HF exchange provide the best prediction of the electronic excited transitions.[17] Interestingly, the M06 global hybrid functional with 27% HF exchange, in contrast with its high general performance in the prediction of thermochemistry, kinetic, bond formation and non-covalent interactions,[60] is not able to calculate well the excited transitions.

Concerning the effect of the basis set, the increment of the basis functions and the addition of the polarization effect from LANL2DZ to *def2*-TZVP gives an important progress in the quantitative prediction of the spectra. The percent improvement related to the basis set in the prediction of the experimental λ_{max} increases from 13.6% with the functional TPSSh up to 64.4% with MPW1PW91 (*cfr*. blue and red columns of the MAPD values in Figure 4), with a mean percent value of 39.6%. The complete set of results is summarized in Table 4.

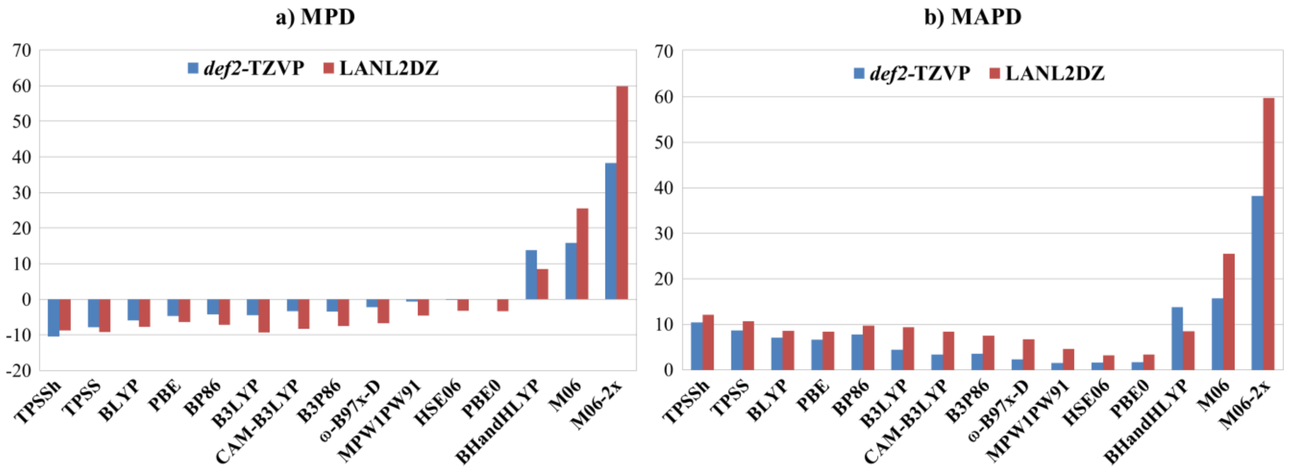

FIGURE 4 Mean percent deviation (MPD) (left) and mean absolute percent deviation (MAPD) (right) from experimental values of λ_{max} determined with fifteen functionals and two basis sets (*def2*-TZVP in blue and LANL2DZ in red).

TABLE 4 Absolute percent deviation (APD), mean absolute percent deviation (MAPD) from the experimental value of λ_{max}, and standard deviations as a function of functional and basis set (D-ζ stands for LANL2DZ and T-ζ for *def2*-TZVP).[a]

Functional	$[Ni(H_{-2}GGC)]^{2-}$		$[Ni(H_{-2}GGG)]^{-}$		$[Ni(H_{-2}GGH)]^{-}$		$[Ni(H_{-3}GGGG)]^{2-}$		$[Ni(trien)]^{2+}$		MAPD (Std. Dev)	
	D-ζ	T-ζ	D-ζ	T-ζ	D-ζ	T-ζ	D-ζ	T-ζ	D-ζ	T-ζ	D-ζ	T-ζ
TPSSh	11.32	9.74	13.46	8.11	8.42	10.06	14.83	13.44	12.60	11.03	12.13 (2.44)	10.47 (1.96)
TPSS	1.94	2.75	14.42	11.37	0.96	0.19	8.76	8.46	16.89	12.68	10.67 (6.30)	8.72 (7.18)
BLYP	4.02	4.06	11.91	10.18	0.77	0.83	10.85	6.73	14.31	11.47	8.59 (7.17)	7.09 (5.43)
PBE	8.56	3.53	10.57	5.58	8.41	3.65	11.64	7.15	7.59	2.46	8.37 (5.71)	6.65 (4.37)
BP86	8.02	2.92	9.74	4.65	7.48	2.62	10.70	6.24	5.94	0.64	9.73 (5.38)	7.76 (3.65)
B3LYP	6.90	2.71	8.60	4.56	6.52	2.72	10.05	6.36	5.59	1.37	9.35 (1.68)	4.47 (1.87)
CAM-B3LYP	6.10	0.79	8.76	3.63	5.36	1.36	9.48	5.03	4.07	0.69	8.38 (1.88)	3.41 (2.12)
B3P86	4.18	0.01	5.93	1.86	3.53	0.19	7.31	3.73	2.14	2.05	7.53 (1.78)	3.55 (1.94)
ω-B97x-D	2.87	0.42	4.26	1.43	2.23	0.59	6.10	3.39	0.77	2.45	6.75 (2.29)	2.30 (1.93)
MPW1PW91	3.05	0.57	4.49	1.27	2.38	0.76	6.25	3.26	0.87	2.71	4.62 (2.03)	**1.57 (1.53)**
HSE06	8.59	14.46	6.37	11.67	10.02	15.08	5.07	9.55	12.42	18.27	3.25 (2.03)	**1.65 (1.26)**
PBE0	21.82	14.93	21.58	14.39	26.97	16.71	17.72	10.67	39.63	22.10	3.41 (2.06)	**1.71 (1.20)**
BHandHLYP	56.48	38.68	63.99	36.76	60.44	39.54	49.36	31.00	68.76	44.99	8.49 (2.92)	13.80 (3.34)
M06	2.25	3.24	12.98	10.71	6.17	5.40	11.83	7.40	15.40	12.06	25.55 (8.53)	15.76 (4.17)
M06-2x	4.18	0.70	14.45	14.08	3.61	1.27	14.08	11.96	17.05	15.58	59.81 (7.39)	38.19 (5.05)

[a] In boldface font the best values are highlighted.

In Figure 5 the comparison between the experimental spectrum with those calculated using the several functionals is shown in the case of $[Ni(H_{-2}GGC)]^{2-}$.

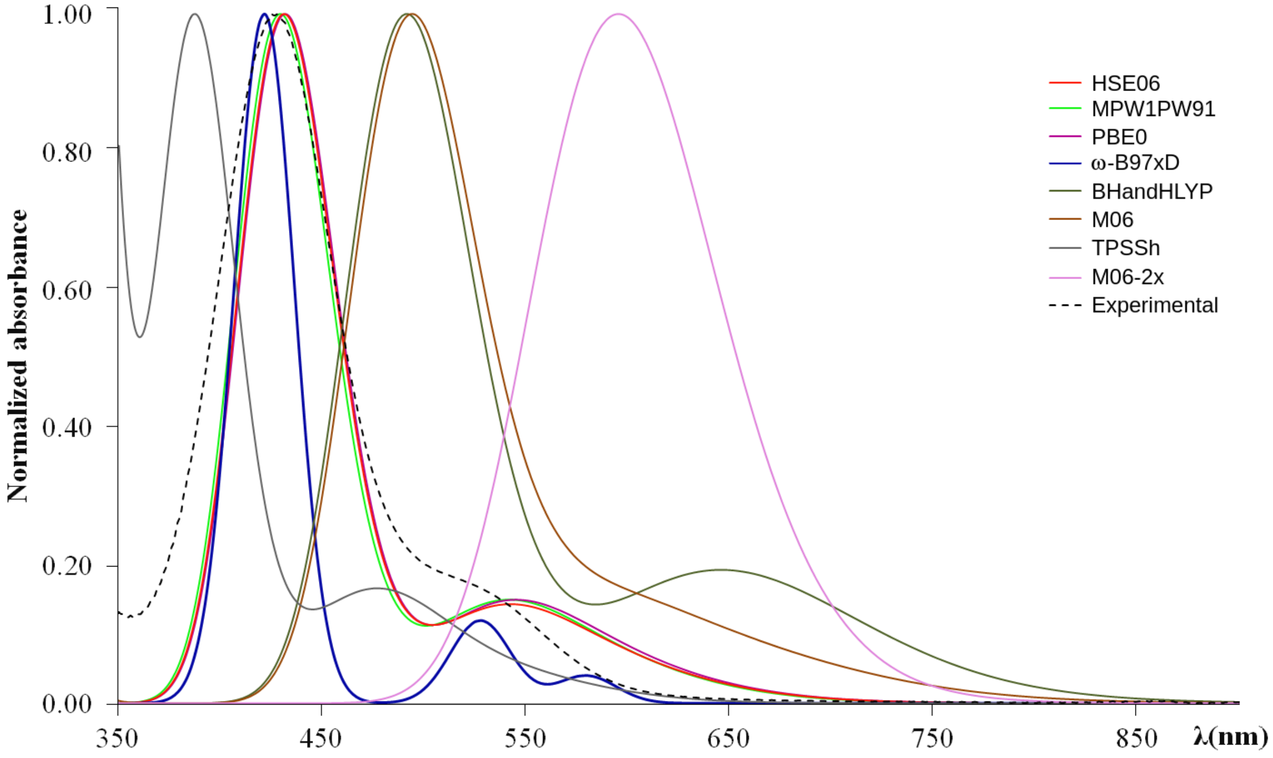

FIGURE 5 Experimental and selected calculated spectra of [Ni(H$_{-2}$GGC)]$^{2-}$ using *def2*-TZVP basis set and several functionals. The absorbance of the spectra was normalized for clarity.

It must be highlighted that TD-DFT electronic vertical excitation energies have been computed using the PCM implicit solvation model on the Linear Response Non-Equilibrium framework (LRNE).[61] Considering that some authors have recently shown that this is not necessarily the best approximation,[62] a Franck-Condon analysis was performed to calculate the vibrational components of the spectrum of [Ni(H$_{-2}$GGC)]$^{2-}$ according to the procedure established by Barone et al. [63]; the Franck-Condon factor $|\langle\Psi_{\mathrm{i}}|\Psi_{\mathrm{f}}\rangle|^2$ less than 10^{-4} indicates that this method is not applicable for our species, probably because the geometry of the excited state – which shows a not negligible deviation from the planarity – is different with respect that of the ground state.

The TD vertical excitations for [Ni(H$_{-2}$GGC)]$^{2-}$ obtained applying the LRNE approach were compared with those obtained with the Linear Response Equilibrium (LRE),[64] State Specific Non-Equilibrium (SSNE)[65] and State Specific Equilibrium (SSE)[65] frameworks (using the HSE06 functional and *def2*-TZVP basis set). The calculated λ_{max} are 429.7 nm (SSNE), 430.8 nm (LRNE), 431.2 nm (LRE) and 432.6 nm (SSE) (vs. the experimental value of 429 nm), indicating a scarce influence of the medium in the excited state stabilization and the good performance of LRNE approximation in the prediction of the absorption wavelength.[66]

Effect of the geometry optimization. The effect of the geometry optimization on the quality of the predicted spectrum was also investigated using [Ni(H$_{-2}$GGC)]$^{2-}$ as benchmark. The structure of the Ni(II) species was optimized with all the fifteen functionals and the electronic transitions were computed on each geometry with the same functional applied for the optimization. Table S6 of Supporting Information lists selected bond lengths and angles (predicted with the basis set *def2*-TZVP), while Table S7 the absolute percent deviation (APD) and percent deviation (PD) from the experimental values of λ_{max}.

The results indicate that, except for the worse functionals (TPSSh, BHandHLYP, M06, and M06-2X), the difference is small and below 3%. For the best functionals (HSE06, MPW1PW91, PBE0, and ω-B97x-D), it is below 1% and B3P86 must be preferred for the optimization. This can be put in relationship with the good performance of this functional in the prediction of the structure of first-row transition metal complexes.[37] In Figure 6 the results obtained in the prediction of λ_{max} for $[Ni(H_{-2}GGC)]^{2-}$ – using B3P86 or each of the other functionals in the optimization step – were compared.

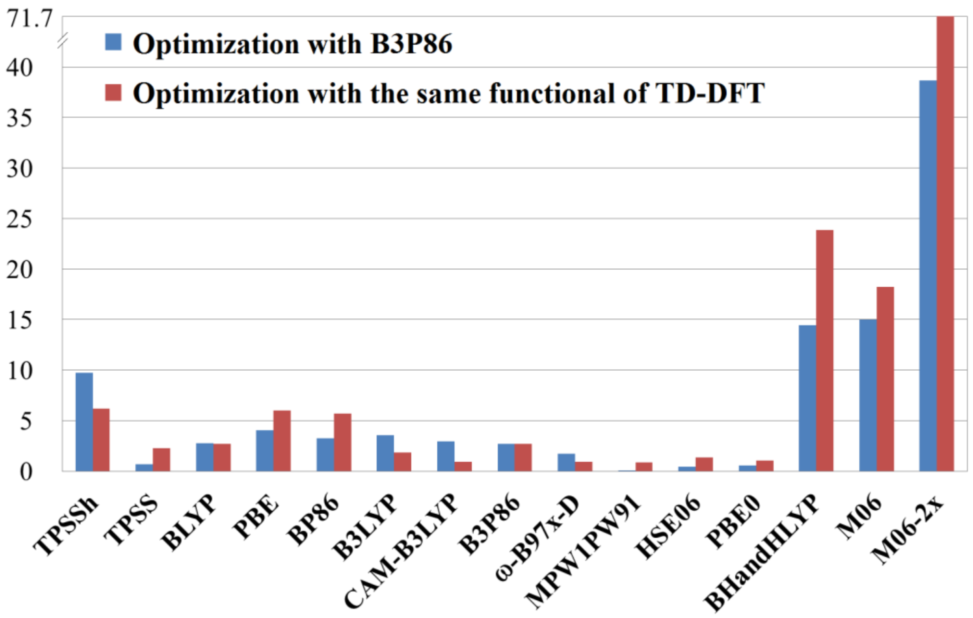

FIGURE 6 Absolute percent deviation (APD) of calculated λ_{max} for $[Ni(H_{-2}GGC)]^{2-}$ from the experimental value, determined with the fifteen functionals at the B3P86 optimized geometries (blue columns) and at the geometries optimized with each functional (red columns).

Nature of the electronic transitions. The nature of the most important vertical electronic transitions in the visible region was also calculated and the data obtained with the functional HSE06 are summarized in Table 5. A given transition can be described in terms of a linear combination of vertical excitations from occupied to virtual MOs and, consequently, only the dominant character of each transition and its contribution can be specified.

TABLE 5 Calculated and experimental transitions (λ_{max}) for the analyzed Ni(II) complexes using the functional HSE06 and the basis-set *def2*-TZVP.

Complex	Transition (% weight)	Main character [a, b]	$\lambda^{calcd\ c}$	f ($\times10^5$) [d]	λ^{exptl} / $\varepsilon^{exptl\ c,e}$
$[Ni(H_{-2}GGC)]^{2-}$	H-12 → L (41.5)	Ni-d_{xy} (62.3) → Ni-$d_{x^2-y^2}$ (52.0)	430.8	300	429 / 338
$[Ni(H_{-2}GGG)]^{-}$	H-7 → L (44.6)	Ni-d_{xy} (43.8) → Ni-$d_{x^2-y^2}$ (61.2)	426.8	400	433 / 287
$[Ni(H_{-2}GGH)]^{-}$	H-11 → L (49.5)	Ni-d_{xy} (67.7) → Ni-$d_{x^2-y^2}$ (60.5)	427.5	160	425 / 198
$[Ni(H_{-3}GGGG)]^{2-}$	H-11 → L (33.4)	Ni-d_{xy} (54.7) → Ni-$d_{x^2-y^2}$ (59.6)	397.1	240	411 / 238
	H-10 → L (30.6)	Ni-d_{yz} (55.7) → Ni-$d_{x^2-y^2}$ (59.6)			
$[Ni(trien)]^{2+}$	H-3 → L (65.0)	Ni-d_{xy} (59.0) → Ni-$d_{x^2-y^2}$ (62.2)	455.9	80	445 / 28

[a] The character of the orbital was assigned considering the largest contribution of the fragment to the specific MO.

[b] Percent contribution of the Ni atomic orbital to the MO.

[c] λ values measured in nm.

[d] Strength of the oscillator associated with the transition.

[e]ε values in M^{-1} cm^{-1}.

Table 5 clearly shows that all the absorptions are due to *d*-*d* transitions and the oscillator strengths are coherent with the experimental values of the molar absorptivity ε; in particular, the oscillator strength for the absorption of $[Ni(trien)]^{2+}$ is significantly lower than those of the species formed by tri- and tetrapeptides, in good agreement with the experiment. It is also obvious that the principal calculated electronic excitation that contributes to the *d*-*d* band is not a HOMO → LUMO transition, but is due to a combination of excitations from occupied MOs having metal character with energy lower than HOMO. As a representative example, the absorption band of $[Ni(H_{-2}GGC)]^{2-}$, predicted at 430.8 nm with HSE06 functional, is a combination of the transitions HOMO-12 → LUMO (41.5%) and HOMO-10 → LUMO (23.4%). The results obtained with other functionals (PBE0, MPW1PW91, ω-B97x-D and M06) are reported in Table S8 of Supporting Information and are comparable. With all the functionals, the absorption in the spectrum of $[Ni(H_{-2}GGC)]^{2-}$ is a composite transition with major contribution deriving from HOMO-12 to LUMO; the percent weight of this transition is 41.7% with PBE0, 43.4% with MPW1PW91, 39.8% with ω-B97x-D, and 48.5% with M06.

The MOs involved in the transitions for all the Ni(II) species are presented in Figure 7.

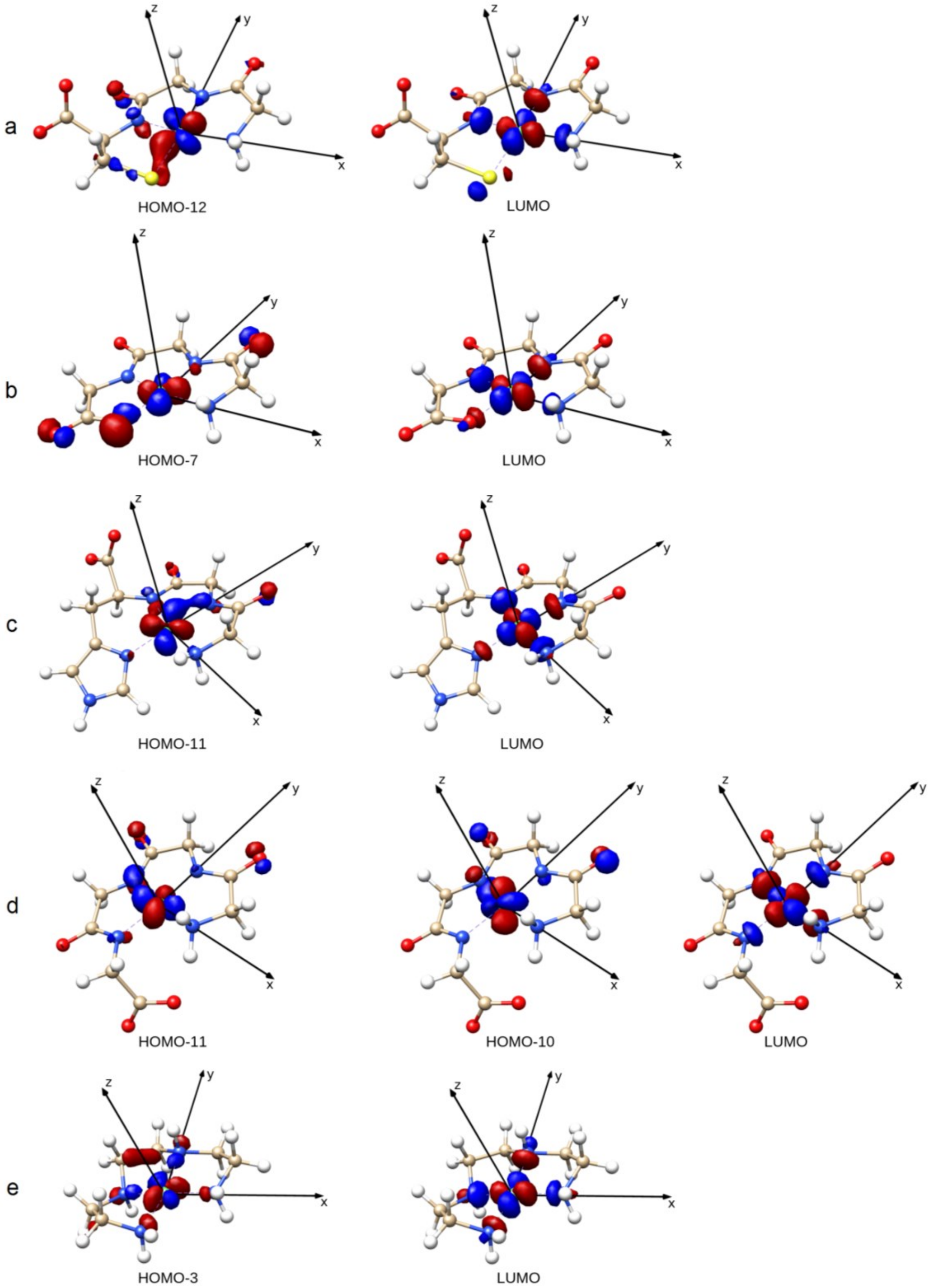

FIGURE 7 Graphical representation of the MOs involved in the TD-DFT calculated transitions (λ_{max}) using the level of theory HSE06/*def2*-TZVP: a) $[Ni(H_{-2}GGC)]^{2-}$; b) $[Ni(H_{-2}GGG)]^{-}$; c) $[Ni(H_{-2}GGH)]^{-}$; d) $[Ni(H_{-3}GGG)]^{2-}$ and e) $[Ni(trien)]^{2+}$.

Prediction of the electronic structure. The electronic structure analysis of the five complexes $[Ni(H_{-2}GGC)]^{2-}$, $[Ni(H_{-2}GGG)]^{-}$, $[Ni(H_{-2}GGH)]^{-}$, $[Ni(H_{-3}GGGG)]^{2-}$ and $[Ni(trien)]^{2+}$ was performed *via* an MPA calculation, setting the *x* and *y* axes in the equatorial plane along the directions Ni–NH_2 and Ni–NR_2, respectively, while the principal symmetry *z* axis was roughly oriented perpendicularly to the *xy* plane as shown in Figure 7. The relative energy levels of the MOs with *d* character are represented in Scheme 2; the energy scale was built for each complex putting the lowest MO as reference at 0.0 eV. The percent contribution, with respect to the total amount of Ni in the specific MO, is reported in parentheses.

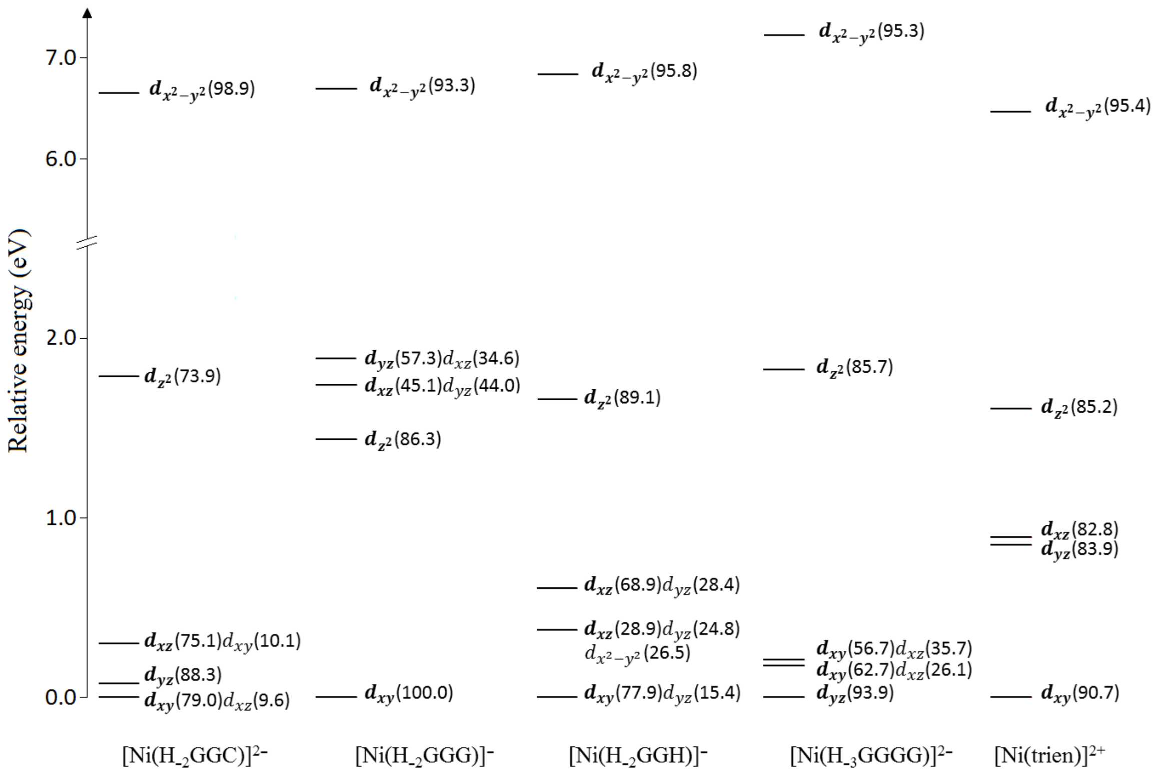

SCHEME 2 Calculated relative energy levels and MO composition of Ni-*d* orbitals for the five complexes $[Ni(H_{-2}GGC)]^{2-}$, $[Ni(H_{-2}GGG)]^{-}$, $[Ni(H_{-2}GGH)]^{-}$, $[Ni(H_{-3}GGGG)]^{2-}$ and $[Ni(trien)]^{2+}$. The energy of the MOs is relative to the value of the most stable orbital set as reference to 0.0 eV. Boldface fonts indicate the main character of the orbital and the values in parentheses the Ni-*d* percent contribution with respect to the total Ni amount in the specific MO.

The order of energy of Ni-*d* atomic orbitals varies with the structure of the species. The results can be summarized as follows: i) the Ni-$d_{x^2-y^2}$ is the *d* orbital at the highest energy, in agreement with the ligand field theory (LFT);[67] ii) the orbital Ni-d_{z^2}, antibonding in an octahedron, is stabilized in a square planar complex where it is only weakly antibonding for the small interactions with the four ligands in the *xy* plane;[67] iii) the three orbitals Ni-d_{xy}, Ni-d_{yz} Ni-d_{xz} have almost the same energy (even if they are not degenerate by symmetry) according to the prediction of the LFT;[67] iv) the splitting between Ni-d_{xz} and Ni-d_{yz} (e_g in D_{4h} symmetry) is negligible and a significant mixing between these two orbitals is expected;[67] v) except for $[Ni(H_{-3}GGGG)]^{2-}$, the MO based on Ni-d_{xy} is the lowest orbital, in agreement with the results obtained for similar square planar Ni(II) structures.[68] In general, the energy order of Ni-*d* orbitals is Ni-d_{xy} ~ Ni-d_{xz} ~ Ni-d_{yz} < Ni-d_{z^2} < Ni-$d_{x^2-y^2}$, the differences with respect to the ideal behavior being attributable to the slight deviations from the regular square planar geometry due to the ligand structure.

The five MOs with *d* character for $[Ni(trien)]^{2+}$ are represented in Figure 8.

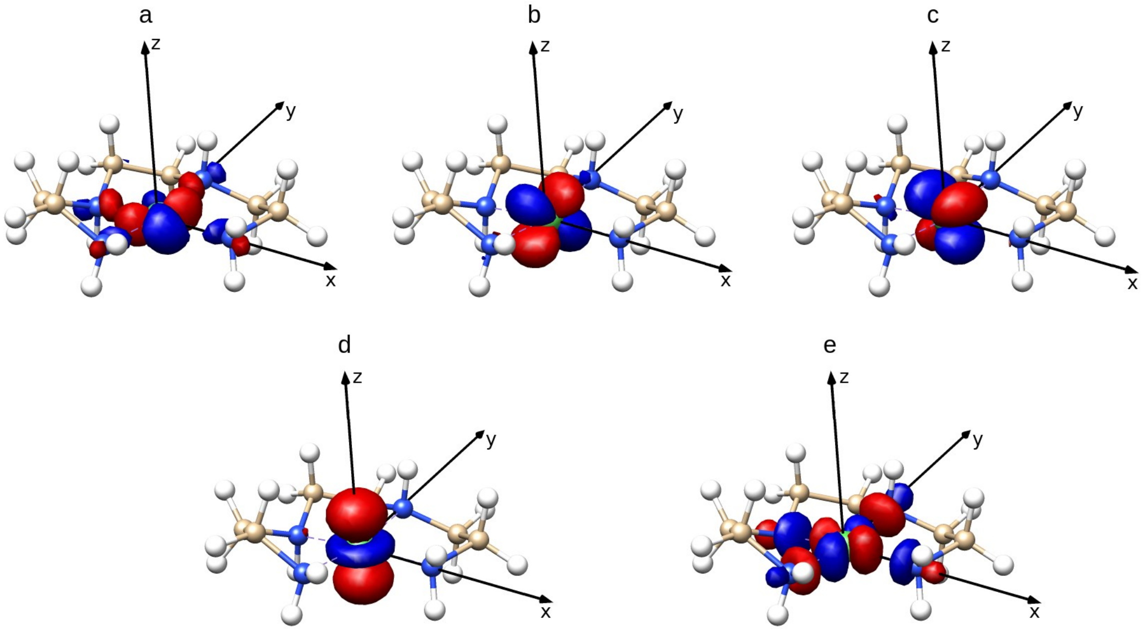

FIGURE 8 MOs for [Ni(trien)]$^{2+}$ with *d* character: (a) HOMO-3 (Ni-d_{xy}); (b) HOMO-2 (Ni-d_{yz}); (c) HOMO-1 (Ni-d_{xz}); (d) HOMO (Ni-d_{z^2}) and (e) LUMO (Ni-$d_{x^2-y^2}$). The position of the three Cartesian axes is also indicated. MOs were calculated at the level of theory HSE06/*def2*-TZVP.

4. CONCLUSIONS

Metal species play a number of roles in chemistry as well as in biology and medicine.[69] Since in most of cases the chemical, biochemical and pharmacological action is related to the type of structure and chemical bond of the metal ion with the ligands or bioligands, in the absence of an X-ray structure other resources are necessary to give insights on the species formed (for example, spectroscopic techniques such as NMR, EPR, UV-vis, IR and CD). Unfortunately, the interpretation of the spectroscopic response is not a trivial task, and many tools have been developed to predict the spectroscopic behavior of a metal complex. Among these tools, computational methods, in particular based on density functional theory (DFT), have been demonstrated very useful and, today, the EPR and NMR spectra of a metal compound can be calculated successfully for a large number of molecules. Up to now, however, the prediction of a UV-vis spectrum is possible only qualitatively and a quantitative agreement has not been reached yet.

Nickel is an element of the first-row transition metals which, as it is known, has both chemical and biological importance. In this study, we have compared the performance of fifteen functionals (among which generalized gradient approximation, global and range-separated hybrids), and two basis sets (one double-ζ and one triple-ζ) in the prediction of the UV-vis spectrum of square planar Ni(II) species, which are characterized by a strong absorption in the visible region. The results indicate that HSE06, MPW1PW91 and PBE0 functionals works better than the other ones and that, using the level of theory HSE06/*def2*-TZVP, the spectrum of a square planar Ni(II) species can be predicted very well. The best performances can be related to the amount of HF exchange in the functional and a value around 25% seems to be the best, larger amount resulting in an overestimation of the experimental absorptions and smaller values in an underestimation. As expected, the effect of the basis set is weaker, and the use of a triple-ζ polarized (*def2*-TZVP) is enough to obtain good results.

The comparison of the data discussed in this study with those available in the literature for Pt(II), Ir(III), Cu(II) and Zn(II) suggests that, in the framework of TD-DFT calculations, it is not possible to propose general computational conditions to get a good agreement between an experimental and a calculated spectrum of the metal complex; in fact, for Pt(II) and Ir(III) species B3LYP and B3PW91 functionals performed better than others,[16] whereas for Cu(II) and Zn(II) complexes B1LYP, B97-2, B97-1, X3LYP, and B98 gave the best results.[17] Therefore, we can conclude that, on the basis of the data in the literature, the best combination of the functional and basis set must be obtained case by case and, up to now, there are no rules to predict which level of theory will give the best agreement with the experiment. In addition, the type of system under examination, restricted and unrestricted, must be taken into account; for example, preliminary results indicate that the level of theory HSE06/*def2*-TZVP is not able to predict accurately the UV-vis spectra of octahedral, paramagnetic Ni(II) complexes. Studies on these systems are in progress in our groups.

ACKNOWLEDGEMENTS

This work was supported by the ÚNKP-17-3 New National Excellence program of the Ministry of Human Capacities, the EU and co-financed by the European Regional Development Fund under the project GINOP-2.3.2-15-2016-000 and the Hungarian Scientific Research Fund (K 124983). A.L., J.-D.M. and G.S. thank the financial support from the Spanish MINECO (project CTQ2017-87889-P). G. S. thanks Universitat Autònoma de Barcelona for the support to his Ph.D. E.G. thanks Fondazione di Sardegna (project FdS15Garribba).

ORCID

Giuseppe Sciortino: 0000-0001-9657-1788
Norbert Lihi: 0000-0003-2986-2395
Jean-Didier Maréchal: 0000-0002-8344-9043
Agustí Lledós: 0000-0001-7909-422X
Eugenio Garribba: 0000-0002-7229-5966

NOTES

The authors declare no competing financial interest.

SUPPORTING INFORMATION

Additional Supporting Information may be found in the online version of this article.

REFERENCES

[1] W. Kohn, L. J. Sham, *Phys. Rev.* **1965**, *140*, A1133-A1138.

[2] F. Neese, *JBIC, J. Biol. Inorg. Chem.* **2006**, *11*, 702-711.

[3] F. Neese, *Coord. Chem. Rev.* **2009**, *253*, 526-563.

[4] A. J. Cohen, P. Mori-Sánchez, W. Yang, *Chem. Rev.* **2012**, *112*, 289-320.

[5] B. Kaduk, T. Kowalczyk, T. Van Voorhis, *Chem. Rev.* **2012**, *112*, 321-370.

[6] A. C. Tsipis, *Coord. Chem. Rev.* **2014**, *272*, 1-29.

[7] N. Mardirossian, M. Head-Gordon, *Mol. Phys.* **2017**, *115*, 2315-2372.

[8] M. G. Medvedev, I. S. Bushmarinov, J. Sun, J. P. Perdew, K. A. Lyssenko, *Science* **2017**, *355*, 49-52.

[9] T. van Mourik, M. Bühl, M.-P. Gaigeot, *Phil. Trans. R. Soc. A* **2014**, *372*, 20120488.

[10] B. Kirste, *Chem. Sci. J.* **2016**, *7*, 127.

[11] a) A. Bagno, F. Rastrelli, G. Saielli, *Chem.–Eur. J.* **2006**, *12*, 5514-5525; b) F. V. Toukach, V. P. Ananikov, *Chem. Soc. Rev.* **2013**, *42*, 8376-8415; c) P. H. Willoughby, M. J. Jansma, T. R. Hoye, *Nat. Protocols* **2014**, *9*, 643-660.

[12] a) A. C. Saladino, S. C. Larsen, *J. Phys. Chem. A* **2003**, *107*, 1872-1878; b) F. Neese, *J. Chem. Phys.* **2003**, *118*, 3939-3948; c) M. L. Munzarová in *Calculation of NMR and EPR Parameters*, *Vol.* (Eds.), Wiley-VCH Verlag GmbH & Co. KGaA, **2004**, pp. 461-482; d) G. Micera, E. Garribba, *J. Comput. Chem.* **2011**, *32*, 2822-2835; e) D. Sanna, G. Sciortino, V. Ugone, G. Micera, E. Garribba, *Inorg. Chem.* **2016**, *55*, 7373-7387.

[13] *Computational Spectroscopy: Methods, Experiments and Applications* (Eds.), Wiley-VCH Verlag GmbH & Co. KGaA, Weinheim, **2010**.

[14] a) M. E. Casida, H. Chermette, D. Jacquemin, *J. Mol. Struct. Theochem* **2009**, *914*, 1-2; b) E. Runge, E. K. U. Gross, *Phys. Rev. Lett.* **1984**, *52*, 997-1000.

[15] a) M. Caricato, B. Mennucci, J. Tomasi, F. Ingrosso, R. Cammi, S. Corni, G. Scalmani, *J. Chem. Phys.* **2006**, *124*, 124520; b) D. Jacquemin, E. A. Perpète, I. Ciofini, C. Adamo, *Acc. Chem. Res.* **2009**, *42*, 326-334; c) D. Jacquemin, A. Planchat, C. Adamo, B. Mennucci, *J. Chem. Theory Comput.* **2012**, *8*, 2359-2372; d) C. Adamo, D. Jacquemin, *Chem. Soc. Rev.* **2013**, *42*, 845-856; e) A. D. Laurent, D. Jacquemin, *Int. J. Quantum Chem.* **2013**, *113*, 2019-2039; f) S. E. Harnung, E. Larsen, *Coord. Chem. Rev.* **2016**, *307*, 81-103; g) D. Padula, S. Jurinovich, L. Di Bari, B. Mennucci, *Chem.–Eur. J.* **2016**, *22*, 17011-17019.

[16] C. Latouche, D. Skouteris, F. Palazzetti, V. Barone, *J. Chem. Theory Comput.* **2015**, *11*, 3281-3289.

[17] J. P. Holland, J. C. Green, *J. Comput. Chem.* **2010**, *31*, 1008-1014.

[18] H. F. Stanyon, X. Cong, Y. Chen, N. Shahidullah, G. Rossetti, J. Dreyer, G. Papamokos, P. Carloni, J. H. Viles, *FEBS J.* **2014**, *281*, 3945-3954.

[19] A. DeFusco, N. Minezawa, L. V. Slipchenko, F. Zahariev, M. S. Gordon, *J. Phys. Chem. Lett.* **2011**, *2*, 2184-2192.

[20] *Inorganic Electronic Structure and Spectroscopy* (Eds.), Wiley, New York, **2006**.

[21] a) E. Lodyga-Chruscinska, D. Sanna, E. Garribba, G. Micera, *Dalton Trans.* **2008**, 4903-4916; b) G. Micera, E. Garribba, *Eur. J. Inorg. Chem.* **2010**, 4697-4710; c) D. Sanna, K. Varnagy, S. Timari, G. Micera, E. Garribba, *Inorg. Chem.* **2011**, *50*, 10328-10341; d) G. Micera, E. Garribba, *Eur. J. Inorg. Chem.* **2011**, 3768-3780; e) L. Pisano, K. Varnagy, S. Timari, K. Hegetschweiler, G. Micera, E. Garribba, *Inorg. Chem.* **2013**, *52*, 5260-5272; f) S. Kundu, D. Mondal, K. Bhattacharya, A. Endo, D. Sanna, E. Garribba, M. Chaudhury, *Inorg. Chem.* **2015**, *54*, 6203-6215; g) S. P. Dash, S. Majumder, A. Banerjee, M. F. N. N. Carvalho, P. Adão, J. Costa Pessoa, K. Brzezinski, E. Garribba, H. Reuter, R. Dinda, *Inorg. Chem.* **2016**, *55*, 1165-1182.

[22] S. Z. Tasker, E. A. Standley, T. F. Jamison, *Nature* **2014**, *509*, 299-309.

[23] a) S. M. Barnett, K. I. Goldberg, J. M. Mayer, *Nat. Chem.* **2012**, *4*, 498-502; b) M. Gao, W. Sheng, Z. Zhuang, Q. Fang, S. Gu, J. Jiang, Y. Yan, *J. Am. Chem. Soc.* **2014**, *136*, 7077-7084; c) Y. Han, Y. Wu, W. Lai, R. Cao, *Inorg. Chem.* **2015**, *54*, 5604-5613.

[24] a) *The Biological Chemistry of Nickel* (Eds.), The Royal Society of Chemistry, Croydon, **2017**; b) *Nickel and its surprising impact in nature* (Eds.), John Wiley & Sons, **2007**; c) J. E. Zweig, D. E. Kim, T. R. Newhouse, *Chem. Rev.* **2017**, *117*, 11680-11752.

[25] L. M. Venanzi, *J. Chem. Soc.* **1958**, 719-724.

[26] a) H. Sigel, R. B. Martin, *Chem. Rev.* **1982**, *82*, 385-426; b) H. Kozłowski, W. Bal, M. Dyba, T. Kowalik-Jankowska, *Coord. Chem. Rev.* **1999**, *184*, 319-346; c) I. Sovago, K. Osz, *Dalton Trans.* **2006**, 3841-3854; d) I. Sóvágó, C. Kállay, K. Várnagy, *Coord. Chem. Rev.* **2012**, *256*, 2225-2233; e) I. Sóvágó, K. Várnagy, N. Lihi, Á. Grenács, *Coord. Chem. Rev.* **2016**, *327*, 43-54.

[27] C. Harford, B. Sarkar, *Acc. Chem. Res.* **1997**, *30*, 123-130.

[28] a) C. E. Jones, M. Klewpatinond, S. R. Abdelraheim, D. R. Brown, J. H. Viles, *J. Mol. Biol.* **2005**, *346*, 1393-1407; b) M. Klewpatinond, J. H. Viles, *FEBS Lett.* **2007**, *581*, 1430-1434; c) D. Valensin, K. Gajda, E. Gralka, G. Valensin, W. Kamysz, H. Kozlowski, *J. Inorg. Biochem.* **2010**, *104*, 71-78.

[29] a) J. G. Kusters, A. H. M. van Vliet, E. J. Kuipers, *Clin. Microbiol. Rev.* **2006**, *19*, 449-490; b) M. Rowinska-Zyrek, D. Witkowska, D. Valensin, W. Kamysz, H. Kozlowski, *Dalton Trans.* **2010**, *39*, 5814-5826; c) D. Witkowska, M. Rowinska-Zyrek, G. Valensin, H. Kozlowski, *Coord. Chem. Rev.* **2012**, *256*, 133-148.

[30] H.-D. Youn, E.-J. Kim, J.-H. Roe, Y. C. Hah, S.-O. Kang, *Biochem. J.* **1996**, *318*, 889-896.

[31] M. A. Siegler, M. Lutz, *Cryst. Growth Des.* **2009**, *9*, 1194-1200.

[32] a) J. Holland, P. J. Barnard, S. R. Bayly, J. Dilworth, J. Green, *Inorg. Chim. Acta* **2009**, *362*, 402-406; b) S. Jana, P. K. Bhaumik, K. Harms, S. Chattopadhyay, *Polyhedron* **2014**, *78*, 94-103; c) L. Liu, M.-W. Shao, X.-H. Wang, *J. Solid State Chem.* **2010**, *183*, 590-594; d) M. Prushan, D. M. Tomezsko a, S. Lofland, M. Zeller c, A. Hunter, *Inorg. Chim. Acta* **2007**, *360*, 2245-2254.

[33] M. J. Frisch, G. W. Trucks, H. B. Schlegel, G. E. Scuseria, M. A. Robb, J. R. Cheeseman, G. Scalmani, V. Barone, B. Mennucci, G. A. Petersson, H. Nakatsuji, M. Caricato, X. Li, H. P. Hratchian, A. F. Izmaylov, J. Bloino, G. Zheng, J. L. Sonnenberg, M. Hada, M. Ehara, K. Toyota, R. Fukuda, J. Hasegawa, M. Ishida, T. Nakajima, Y. Honda, O. Kitao, H. Nakai, T. Vreven, J. A. Montgomery, Jr., J. E. Peralta, F. Ogliaro, M.

Bearpark, J. J. Heyd, E. Brothers, K. N. Kudin, V. N. Staroverov, T. Keith, R. Kobayashi, J. Normand, K. Raghavachari, A. Rendell, J. C. Burant, S. S. Iyengar, J. Tomasi, M. Cossi, N. Rega, J. M. Millam, M. Klene, J. E. Knox, J. B. Cross, V. Bakken, C. Adamo, J. Jaramillo, R. Gomperts, R. E. Stratmann, O. Yazyev, A. J. Austin, R. Cammi, C. Pomelli, J. W. Ochterski, R. L. Martin, K. Morokuma, V. G. Zakrzewski, G. A. Voth, P. Salvador, J. J. Dannenberg, S. Dapprich, A. D. Daniels, Ö. Farkas, J. B. Foresman, J. V. Ortiz, J. Cioslowski, D. J. Fox, *Gaussian 09, revision D.01*, Gaussian, Inc., Wallingford, CT, **2010**.

[34] A. D. Becke, *J. Chem. Phys.* **1993**, *98*, 5648-5652.

[35] a) J. P. Perdew, *Phys. Rev. B* **1986**, *33*, 8822-8824; b) J. P. Perdew, *Phys. Rev. B* **1986**, *34*, 7406-7406.

[36] a) R. Cammi, J. Tomasi, *J. Comput. Chem.* **1995**, *16*, 1449-1458; b) S. Miertuš, E. Scrocco, J. Tomasi, *Chem. Phys.* **1981**, *55*, 117-129.

[37] a) M. Bühl, H. Kabrede, *J. Chem. Theory Comput.* **2006**, *2*, 1282-1290; b) M. Bühl, C. Reimann, D. A. Pantazis, T. Bredow, F. Neese, *J. Chem. Theory Comput.* **2008**, *4*, 1449-1459.

[38] a) G. Micera, V. L. Pecoraro, E. Garribba, *Inorg. Chem.* **2009**, *48*, 5790-5796; b) G. Micera, E. Garribba, *Int. J. Quantum Chem.* **2012**, *112*, 2486-2498; c) D. Sanna, P. Buglyo, L. Biro, G. Micera, E. Garribba, *Eur. J. Inorg. Chem.* **2012**, 1079-1092; d) D. Sanna, V. Ugone, G. Micera, E. Garribba, *Dalton Trans.* **2012**, *41*, 7304-7318; e) D. Sanna, P. Buglyo, A. I. Tomaz, J. C. Pessoa, S. Borovic, G. Micera, E. Garribba, *Dalton Trans.* **2012**, *41*, 12824-12838; f) D. Sanna, K. Várnagy, N. Lihi, G. Micera, E. Garribba, *Inorg. Chem.* **2013**, *52*, 8202-8213.

[39] C. Lee, W. Yang, R. G. Parr, *Phys. Rev. B* **1988**, *37*, 785-789.

[40] T. Yanai, D. P. Tew, N. C. Handy, *Chem. Phys. Lett.* **2004**, *393*, 51-57.

[41] J.-D. Chai, M. Head-Gordon, *J. Chem. Phys.* **2008**, *128*, 084106.

[42] C. Adamo, V. Barone, *J. Chem. Phys.* **1998**, *108*, 664-675.

[43] A. V. Krukau, O. A. Vydrov, A. F. Izmaylov, G. E. Scuseria, *J. Chem. Phys.* **2006**, *125*, 224106.

[44] a) J. P. Perdew, K. Burke, M. Ernzerhof, *Phys. Rev. Lett.* **1996**, *77*, 3865-3868; b) J. P. Perdew, K. Burke, M. Ernzerhof, *Phys. Rev. Lett.* **1997**, *78*, 1396-1396.

[45] a) J. Tao, J. P. Perdew, V. N. Staroverov, G. E. Scuseria, *Phys. Rev. Lett.* **2003**, *91*, 146401; b) V. N. Staroverov, G. E. Scuseria, J. Tao, J. P. Perdew, *J. Chem. Phys.* **2003**, *119*, 12129-12137.

[46] Y. Zhao, D. G. Truhlar, *J. Chem. Phys.* **2006**, *125*, 194101.

[47] A. D. Becke, *Phys. Rev. A* **1988**, *38*, 3098-3100.

[48] A.-R. Allouche, *J. Comput. Chem.* **2011**, *32*, 174-182.

[49] a) S. I. Gorelsky, *AOMix: Program for Molecular Orbital Analysis* http://www.sg-chem.net/, version 6.52, 2011; b) S. I. Gorelsky, A. B. P. Lever, *J. Organomet. Chem.* **2001**, *635*, 187-196.

[50] C. Gábor Ágoston, Z. Miskolczy, Z. Nagy, I. Sóvágó, *Polyhedron* **2003**, *22*, 2607-2615.

[51] R. B. Martin, M. Chamberlin, J. T. Edsall, *J. Am. Chem. Soc.* **1960**, *82*, 495-498.

[52] R. W. Hay, M. M. Hassan, C. You-Quan, *J. Inorg. Biochem.* **1993**, *52*, 17-25.

[53] H. Kozlowski, B. D.-L. Révérend, D. Ficheux, C. Loucheux, I. Sovago, *J. Inorg. Biochem.* **1987**, *29*, 187-197.

[54] H. C. Freeman, J. M. Guss, R. L. Sinclair, *Chem. Commun.* **1968**, 485-487.

[55] W. Bal, M. I. Djuran, D. W. Margerum, E. T. Gray, M. A. Mazid, R. T. Tom, E. Nieboer, P. J. Sadler, *J. Chem. Soc., Chem. Commun.* **1994**, 1889-1890.

[56] A. McPherson, M. G. Rossmann, D. W. Margerum, M. R. James, *J. Coord. Chem.* **1971**, *1*, 39-46.

[57] a) Z. Bihari, V. Ugone, E. Garribba, N. Lihi, P. Buglyó, *J. Organomet. Chem.* **2016**, *823*, 116-125; b) L. Bíró, A. J. Godó, Z. Bihari, E. Garribba, P. Buglyó, *Eur. J. Inorg. Chem.* **2013**, *2013*, 3090-3100.

[58] K. Cherifi, B. D.-L. Reverend, C. Loucheux, K. Varnagy, T. Kiss, I. Sovago, H. Kozlowski, *J. Inorg. Biochem.* **1990**, *38*, 69-80.

[59] a) S. Grimme, C. Mück-Lichtenfeld, E.-U. Würthwein, A. W. Ehlers, T. P. M. Goumans, K. Lammertsma, *J. Phys. Chem. A* **2006**, *110*, 2583-2586; b) T. Schwabe, S. Grimme, *Phys. Chem. Chem. Phys.* **2006**, *8*, 4398-4401; c) T. Schwabe, S. Grimme, *Phys. Chem. Chem. Phys.* **2007**, *9*, 3397-3406; d) T. Schwabe, S. Grimme, *Acc. Chem. Res.* **2008**, *41*, 569-579.

[60] a) Y. Zhao, D. G. Truhlar, *Theor. Chem. Acc.* **2008**, *120*, 215-241; b) Y. Zhao, D. G. Truhlar, *Acc. Chem. Res.* **2008**, *41*, 157-167.

[61] R. Cammi, B. Mennucci, J. Tomasi, *J. Phys. Chem. A* **2000**, *104*, 5631-5637.

[62] R. Rüger, T. Niehaus, E. v. Lenthe, T. Heine, L. Visscher, *J. Chem. Phys.* **2016**, *145*, 184102.

[63] V. Barone, J. Bloino, M. Biczysko, F. Santoro, *J. Chem. Theory Comput.* **2009**, *5*, 540-554.

[64] J. Tomasi, B. Mennucci, R. Cammi, *Chem. Rev.* **2005**, *105*, 2999-3094.

[65] R. Cammi, S. Corni, B. Mennucci, J. Tomasi, *J. Chem. Phys.* **2005**, *122*, 104513.

[66] F. Peccati, M. Wisniewska, X. Solans-Monfort, M. Sodupe, *Phys. Chem. Chem. Phys.* **2016**, *18*, 11634-11643.

[67] Y. Jean, *Molecular Orbitals of Transition Metals*, Oxford University Press, Oxford, **2005**.

[68] R. Carrasco, J. Cano, X. Ottenwaelder, A. Aukauloo, Y. Journaux, R. Ruiz-Garcia, *Dalton Trans.* **2005**, 2527-2538.

[69] D. Rehder, *Bioinorganic Chemistry*, Oxford University Press, Oxford, **2014**.

GRAPHICAL ABSTRACT

AUTHOR NAMES: Giuseppe Sciortino, Norbert Lihi, Tamás Czine, Jean-Didier Maréchal, Agustí Lledós, Eugenio Garribba

TITLE: Accurate prediction of vertical electronic transitions of Ni(II) coordination compounds via Time Dependent DFT

TEXT: Fifteen functionals and two basis sets were compared in the prediction of the UV-vis spectra of square planar Ni(II) species. The level of theory HSE06/*def2*-TZVP allows predicting the absorption in the visible region with a mean absolute percent deviation below 2%.

GRAPHICAL ABSTRACT FIGURE